XLIII CILAMCE
21–25, November, 2022
FOZ DO IGUAÇU – PR – BRAZIL

Nonlinear geometric analysis of orthotropic laminated plates and shells with zig-zag effect

Vinícius B. Souza[1], Humberto B. Coda[1]

[1]*Dept. of Structural Engineering, São Carlos School of Engineering, University of São Paulo*
Av. Trab. São Carlense, 400, 13566-590, São Paulo/São Carlos, Brazil
vbarros@usp.br, hbcoda@sc.usp.br

Abstract. In this study, a positional Finite Element Method (FEM) formulation is applied to simulate orthotropic symmetric laminated plates and shells. Alternatively to the traditional FEM, the positional formulation uses a total Lagrangian description based on generalized vectors and nodal positions, providing an inherently nonlinear geometric formulation. However, basic kinematics are not able to satisfy a continuous stress distribution along the laminate thickness. The stress discontinuity is related to the emergence of a zig-zag displacement profile in the transverse direction caused by mechanical properties changing between adjacent laminas. Therefore, the proposed formulation introduces new degrees of freedom to regularize the classical Reissner-Mindlin kinematics and reproduce the zig-zag effect. In addition, the mechanical model uses Green-Lagrange strain and the Saint Venant-Kirchhoff constitutive law, which allows moderate strain. A numerical example is employed to validate the proposed formulation and demonstrate its quality when compared with literature results.

Keywords: laminated plates and shells, zig-zag effect, orthotropic material, positional FEM.

1 Introduction

Composite materials have been used as alternative substitutes for conventional materials (e.g. metal and wood) as a strategy to introduce additional flexibility to designs and provide better engineering properties. There are commonly three types of composite materials according to Reddy [1]; one of them are the laminates. Laminated composites are formed by combining different materials in layers of generally uniform thickness, also called lamina or ply, overlapped and adhered to each other along the transverse direction.

At the end of the manufacturing process, each lamina presents a material with homogeneous characteristics on a macroscopic scale and mechanical properties superior to those of its constituents. This configuration provides high values of strength and stiffness per unit mass of the structural element, whose characteristics are desirable in the construction, automotive, and aerospace industries. In some cases, the mechanical properties may also change as a function of direction, for example, in orthotropic, anisotropic, and fiber-reinforced laminated materials.

Due to the discontinuity of mechanical properties in the transverse direction, the displacement field may present a sudden change of inclination at the interface of each lamina along the thickness, so-called “zig-zag effect” [2]. According to Coda et al. [3], based on the results of Carrera and Ciuffreda [2], the influence of the zig-zag effect is more important in thick laminated plates, or when the ratio between the length and height of the plate is smaller than 5 or the ratio between the stiffness of laminas is large. Nevertheless, special attention is paid to the analysis of the mechanical behavior of laminated structures, since some theories are not able to satisfy the continuity of transverse stresses in interlaminar regions.

According to Oh et al. [4], the theories for mechanical analysis of laminated shells are divided into three categories: smeared theories, layerwise theories and simplified zig-zag theories. The first are examples of theories that cannot satisfy a continuous distribution of transverse stresses between laminas. The second, the layerwise theories (LW), are able to model the zig-zag effect and adequately predict the local strains and stresses through thickness since they employ layer-dependent degrees of freedom. However, their computational cost becomes high as the number of layers increases. In contrast, the third category employs a zig-zag profile of displacement which

provides accurate analysis of the strain and stress fields with few degrees of freedom, as well as ensuring free tensile conditions on top and bottom surfaces between laminas [4,5]. Because of these advantages, the present study combines the simplified zig-zag theories with the FEM positional formulation.

This combination is not new. Coda et al. [3] regularized the transverse stresses in laminated plates and shells without any new degree of freedom by using the zig-zag mode enrichment of Green's strain tensor. The formulation uses a kinematics similar to that of Reissner-Mindlin, however, to compensate the lack of a new degree of freedom the kinematics has been enhanced by a pre-processor that uses a simple supported beam element. More recently, Coda et al. [6] improved the zig-zag enrichment by introducing new degrees of freedom for laminated or functionally graded two-dimensional beams developing small and large strain. Unlike the previous work [3], Coda et al. [6] eliminated the dependence of the positions of adjacent interfaces on the center of stiffness, thus eliminating the zig-zag effect in homogeneous sections modeled with numerical laminas.

As an extension of the methodology proposed by Coda et al. [6], the present work presents a positional formulation of the FEM for orthotropic laminated plates and shells that includes the regularization of transversal stresses and the zig-zag effect as degrees of freedom. In addition, an enrichment along the transverse direction is introduced into the kinematics to allow linear variation in thickness and eliminate the volumetric locking of the cross section in the current configuration. The proposed formulation is a cinematically exact description and geometrically nonlinear total Lagrangian approach in FEM. To testify the potential of the proposed formulation, a numerical example is tested and compared with the semi-analytical results.

2 The Positional Finite Element Method

The positional formulation of the FEM, originally conceived by Bonet et al. [7] for fluid-supported membrane analysis and later extended by Coda [8] for solid mechanics applications, uses nodal positions and generalized vectors as nodal variables instead of displacements and rotations. The approach presented in this section is based on Coda [9], whose reference is recommended for further details.

2.1 Basic formulation

Differently to the classical Reissner-Mindlin kinematics, in the positional formulation the shell or plate thickness can vary along the equilibrium path. Therefore, the basic formulation can be classified as solid-like kinematics [3]. To allow linear variation of the thickness in the currently configuration, an initial enrichment is introduced in the basic formulation through nodal parameter T. It avoids the “thickness locking”, as described by Bischoff and Ramm [10].

Considering the shell (or plate) reference surface coincident with the stiffness center of the cross section, the mapping functions depicted in Figure 1 at the initial ($\vec{f}^0$) and current ($\vec{f}^1$) positions are:

$$f_i^{0k}(\xi_1,\xi_2,\xi_3) = \phi_\alpha(\xi_1,\xi_2)X_{\alpha i} + \left(d^k + \frac{h_0^k}{2}\xi_3^k\right)\phi_z(\xi_1,\xi_2)V_{zi}\,, \tag{1}$$

$$f_i^{1k}(\xi_1,\xi_2,\xi_3) = \phi_\alpha(\xi_1,\xi_2)Y_{\alpha i} + \left[\left(d^k + \frac{h_0^k}{2}\xi_3^k\right) + \phi_\gamma(\xi_1,\xi_2)T_\gamma\left(d^k + \frac{h_0^k}{2}\xi_3^k\right)^2\right]\phi_z(\xi_1,\xi_2)G_{zi}\,, \tag{2}$$

in which k represents a lamina of thickness h_0^k, d^k is the distance from the mid surface of lamina k to the reference surface, $X_{\alpha i}$ is the i-th initial coordinate of node α and $Y_{\alpha i}$ is the i-th current coordinate of node α, whose value is unknown. $\vec{V}$ is the generalized vector in the initial configuration (unitary and normal to the reference surface) and $\vec{G}$ is the generalized vector in the currently configuration (without restrictions). The Lagrangian shape function ϕ_α related to node α is evaluated in the dimensionless coordinates ξ_1 and ξ_2 from the reference surface mapping (Fig. 1). The isoparametric domain is completed with the dimensionless coordinate ξ_3^k, which is related to the thickness of lamina k.

The total deformation function $\vec{f}$ that describes the configuration changing is given, for each lamina, by:

$$\vec{f}^k = \vec{f}^{1k} \circ (\vec{f}^{0k})^{-1}\,. \tag{3}$$

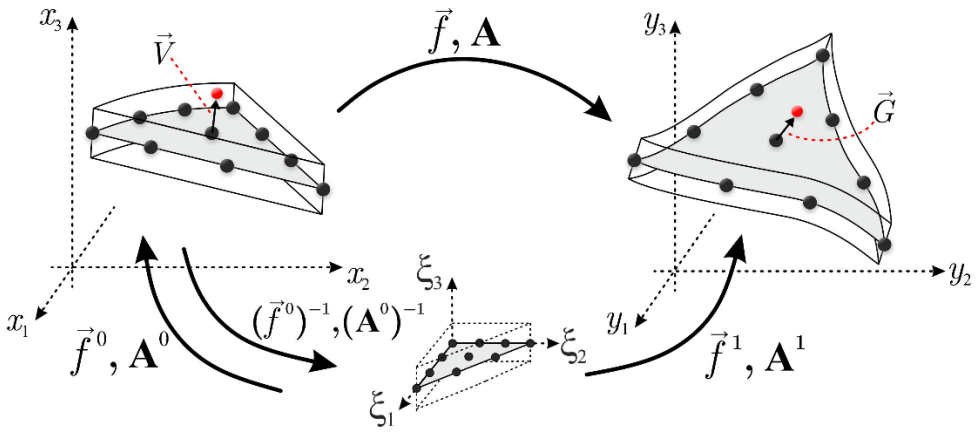

Figure 1. Mapping the initial and current configurations (omitting laminas)

The gradient of Equation (3) can be written, for each lamina, as:

$$\mathbf{A}^k = \nabla(\vec{f}^k) = \mathbf{A}^{1k} \cdot (\mathbf{A}^{0k})^{-1}, \tag{4}$$

in which:

$$\mathrm{A}_{ij}^{0k} = \frac{\partial f_i^{0k}}{\partial \xi_j} \text{ and } \mathrm{A}_{ij}^{1k} = \frac{\partial f_i^{1k}}{\partial \xi_j}. \tag{5}$$

At this point, the basic formulation has six known nodal values in the initial configuration (stored in $\vec{X} = \{X_1, X_2, X_3, V_1, V_2, V_3\}^t$) and seven unknown degrees of freedom by node in the current configuration (stored in $\vec{Y} = \{Y_1, Y_2, Y_3, G_1, G_2, G_3, T\}^t$). In the case of orthotropic material these degrees of freedom are transformed to the orthotropic direction according to the following:

$$\vec{\bar{X}} = \mathbf{R}^t \vec{X} \text{ and } \vec{\bar{Y}} = \mathbf{R}^t \vec{Y}, \tag{6}$$

where $\mathbf{R}$ is the rotation matrix, and $\vec{\bar{X}}$ and $\vec{\bar{Y}}$ are the vectors in the local direction.

2.2 The zig-zag enrichment

The proposed enrichment is included in the $\vec{f}^1$ mapping function by introducing the zig-zag mode $a_{ik}z_{(k)} + b_{ik}$ in Eq. (2), where a_{ik} and b_{ik} are constants of straight lines for the k-th lamina, $i = 1,2$ are the orthotropy directions and $z_k = d^k + (h_0^k/2)\xi_3^k$. The values of a_{ik} and b_{ik} are determined only once for a cross section by imposing the compatibility and equilibrium conditions between adjacent laminas presented by Coda et al. [6]. For symmetrically laminated plates and shells, one writes:

$$\begin{aligned} f_i^{1k}(\xi_1,\xi_2,\xi_3) = \phi_\alpha(\xi_1,\xi_2)Y_{\alpha i} + \left[z_k(\xi_3^k) + \phi_\gamma(\xi_1,\xi_2)T_\gamma(z_k)^2 \right]\phi_z(\xi_1,\xi_2)G_{zi} + \\ + \phi_m(\xi_1,\xi_2)Z_m^1\left[a_{1k}z_{(k)} + b_{1k} \right]\phi_j(\xi_1,\xi_2)\bar{G}_{ji}^1 + \phi_n(\xi_1,\xi_2)Z_n^2\left[a_{2k}z_{(k)} + b_{2k} \right]\phi_p(\xi_1,\xi_2)\bar{G}_{pi}^2, \end{aligned} \tag{7}$$

in which Z_α^i is a new degree of freedom (the intensity of the zig-zag mode) at node α following the orthotropy direction i. $\bar{G}^1$ and $\bar{G}^2$ are vectors orthogonal to the generalized vector and following the orthotropy directions.

In order to smooth the stress distribution, the next deductions are described for a small displacement problem (with rotation θ and internal points displacements d_1). The calculation of shear stress in a horizontal beam developing small displacements, considering the horizontal equilibrium of parts of the cross section, is given by:

$$\tau^k = \int_{z_k}^{z_1^{top}} E_k z_{(k)} \phi_i^{"k} \theta_i + E_k \phi_j^{"k} Z_j \left[a_k z_{(k)} + b_k \right] dz, \tag{8}$$

where E_k is the longitudinal Young modulus of a lamina k and z_1^{top} is the upper limit of the cross section.

Solving Equation (8) and dividing the result by the shear elastic modulus of lamina k (G^k), one provides the distortion $\gamma^k = \tau^k \,/\, G^k$, i.e.:

$$\gamma^k = \left[A_k + C_k(z_k^{top})^2 - C_k z_k^2 \right]\phi_j^{"}(\xi)\theta_j + \{F_k + I_k\left[(z_k^{top})^2 - z_k^2\right] + L_k + M_k(z_k^{top} - z_k)\}\,\phi_p^{"}(\xi)Z_p\,, \quad (9)$$

whose constants are ($\bar{x}$ is the distance from the base of the cross section to the midline of the lamina):

$$\begin{gathered} A_k = \frac{1}{G^k}\sum_{i=k+1}^{n} E_i\bar{x}_i h_0^i,\;\; F_k = \frac{1}{G^k}\sum_{i=k+1}^{n} E_i a_i\bar{x}_i h_0^i,\;\; L_k = \frac{1}{G^k}\sum_{i=k+1}^{n} E_i b_i h_0^i\,, \\ C_k = \frac{E_k}{2G^k},\;\; I_k = \frac{E_k a_k}{2G^k},\;\; M_k = \frac{E_k b_k}{G^k}. \end{gathered} \quad (10)$$

Integrating Equation (9) following the z transverse direction of the cross section, the horizontal displacement profile $\bar{d}_1$ is obtained, in which the upper bar indicates a scaling to be introduced. Solving the scale problem, the following expression can be written for small displacements:

$$d_1^k = \phi_\alpha(\xi_1,\xi_2)U_{\alpha i} + u_1^k(z)\phi_l(\xi_1,\xi_2)\theta_l + u_2^k(z)\phi_j(\xi_1,\xi_2)Z_j\,, \quad (11)$$

with $U_{\alpha i} = Y_{\alpha i} - X_{\alpha i}$, and:

$$\begin{aligned} u_1^k(z) &= A_k z + C_k\left[(z_k^{top})^2 - \frac{z^2}{3}\right]z\,, \\ u_2^k(z) &= (F_k + L_k)z + I_k\left[(z_k^{top})^2 - \frac{z^2}{3}\right]z + M_k\left[z_k^{top} - \frac{z}{2}\right]z\,. \end{aligned} \quad (12)$$

In order to introduce Equation (11) in the geometrically non linear kinematics, one subtracts z_k from the term u_1^k to preserve rigid body movements. This is performed in both orthotropy directions by introducing the difference term $r_i^k = u_1^{ik} - z_k$, generating the new degree of freedom R_α^i at node α of the directions $i = 1,2$. From these considerations, Eq. (7) is rewritten as:

$$\begin{aligned} f_i^{1k}(\xi_1,\xi_2,\xi_3) = \phi_\alpha(\xi_1,\xi_2)Y_{\alpha i} &+ \left[z_k(\xi_3^k) + \phi_\gamma(\xi_1,\xi_2)T_\gamma(z_k)^2\right]\phi_z(\xi_1,\xi_2)G_{zi} + \\ &+ \left[r_1^k(\xi_3^k)\phi_m(\xi_1,\xi_2)R_m^1 + u_2^{1k}(\xi_3^k)\phi_s(\xi_1,\xi_2)Z_s^1\right]\phi_j(\xi_1,\xi_2)\bar{G}_{ji}^1 + \\ &+ \left[r_2^k(\xi_3^k)\phi_n(\xi_1,\xi_2)R_n^2 + u_2^{2k}(\xi_3^k)\phi_l(\xi_1,\xi_2)Z_l^2\right]\phi_p(\xi_1,\xi_2)\bar{G}_{pi}^2\,. \end{aligned} \quad (13)$$

Therefore, introducing R_α^i (called here regularization) and Z_α^i (zig-zag) in the $\vec{f}^1$ mapping function the enhanced kinematics has 11 degrees of freedom by node α ($\vec{Y}_\alpha = \{Y_{\alpha1}, Y_{\alpha2}, Y_{\alpha3}, G_{\alpha1}, G_{\alpha2}, G_{\alpha3}, T_\alpha, R_\alpha^1, R_\alpha^2, Z_\alpha^1, Z_\alpha^2\}^t$).

2.3 Equilibrium equations and numerical solution

In the positional FEM, the equilibrium equation is based on the minimization of the total mechanical energy (Π), called Principle of Stationary Mechanical Energy. Focusing on static analysis, i.e. considering only the portions of total strain energy $\mathbb{U}$ and potential energy of external forces $\mathbb{P}$, this principle is written as:

$$\frac{\partial\Pi}{\partial\vec{Y}} = \frac{\partial\mathbb{U}}{\partial\vec{Y}} + \frac{\partial\mathbb{P}}{\partial\vec{Y}} = \vec{0}, \quad (14)$$

where:

$$\frac{\partial\mathbb{U}}{\partial\vec{Y}} = \int_{V_0}\mathbf{S} : \frac{\partial\mathbf{E}}{\partial\vec{Y}}\,\mathrm{d}V_0\,, \quad (15)$$

$$\frac{\partial\mathbb{P}}{\partial\vec{Y}} = -\int_{A_0} q_{i\alpha}^0\phi_\alpha(\xi_1,\xi_2)\phi_\gamma(\xi_1,\xi_2)\mathrm{dA}_0\,, \quad (16)$$

in which $\mathbf{S} = \mathfrak{C} : \mathbf{E}$ is the second Piola-Kirchhoff stress tensor, $\mathbf{E}$ is the Green-Lagrange strain tensor, $\mathfrak{C}$ is the constitutive tensor for orthotropic material, $q_{i\alpha}^0$ is the superficial conservative load distributed in node α of the

direction i, A_0 is the reference surface area, V_0 is the plate or shell volume, and the index "0" indicates the Lagrangian description of the formulation.

The system of equations obtained from Eq. (14) is nonlinear regarding nodal parameters $\vec{Y}$. The strategy adopted here to solve this system is the Newton-Raphson iterative method. Concisely, the Newton-Raphson procedure is described as follows: one chooses a trial solution $\vec{Y}_0$ and calculates the unbalanced force vector $\vec{g}(\vec{Y}_0)$ according to Eq. (17). By applying Eq. (18) one finds the variation of position $\Delta\vec{Y}$ that corrects $\vec{Y}_0$. With this new position vector, the procedure is repeated until the error (Er) becomes smaller than the adopted tolerance (Eq. 19).

$$\vec{g}(\vec{Y}) = \frac{\partial \Pi}{\partial \vec{Y}}, \tag{17}$$

$$\Delta \vec{Y} = -(\mathbf{H})^{-1}\, \vec{g}(\vec{Y}_0), \tag{18}$$

$$Er = \frac{\left|\Delta \vec{Y}\right|}{\left|\vec{Y}_0\right|} < tol, \tag{19}$$

where $\mathbf{H}$ is the Hessian matrix and tol is the tolerance.

After determining the solution that satisfies the stopping criterion (Eq. 19), the Cauchy stress tensor $\boldsymbol{\sigma}$ can be calculated by the following relation:

$$\boldsymbol{\sigma} = \frac{\mathbf{A}\cdot\mathbf{S}\cdot\mathbf{A}^t}{\det(\mathbf{A})}. \tag{20}$$

3 Numerical example: Cross-ply plate loaded by transverse constant pressure

A simply supported square plate (Figure 2) is subjected to a uniform transverse load q. The plate is composed of 3 laminas of the same thickness ($h/3$) with symmetrical ply arrangement (0/90/0), in which 0 indicates that the orthotropic direction 1 coincides with x_1 axis and 90 indicates that direction 1 coincides with x_2 axis.

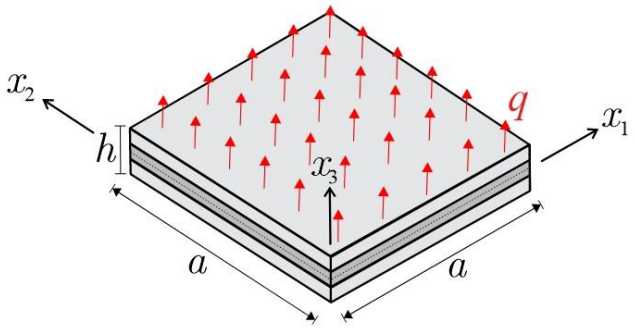

Figure 2. Square laminated plate subjected to surface distributed load

Each lamina is composed by orthotropic material with the following properties: E_1= 200 GPa, E_2=E_3= 8 GPa, G_{12}=G_{13}= 4 GPa, G_{23}= 1.6 GPa and ν_{12}= ν_{13}= ν_{23}= 0.25. Using the adopted values, the example comprises the cases of thick ($a/h = 4$) and thin ($a/h = 100$) plates. In order to compare the numerical results with the semi-analytical solution presented by Carrera and Ciuffreda [2], the parameter T is constrained and equal to zero to ensure no variation of the plate thickness. In addition, the transverse displacement (U_z) and the normal and shear stresses (σ_{11}, σ_{13}) are given in normalized form, according to the expressions:

$$\bar{U}_z = \frac{100 U_z E_2 h^3}{q a^4}, \bar{\sigma}_{11} = \frac{\sigma_{11}}{q(a\ /\ h)^2}, \bar{\sigma}_{13} = \frac{\sigma_{13}}{q(a\ /\ h)}, \tag{21}$$

in which σ_{ij} is measured at the point $(x_1, x_2, \bar{x}_3)$ throughout the normalized thickness $\bar{x}_3 = (x_3 - h/2)/h$.

The entire plate was discretized with a structured mesh of $8x8$ triangular cubic finite elements (128 elements and 625 nodes). Two kinematics are analyzed, denoted by the following acronyms:

- RZ0: basic kinematics (without regularization and zig-zag enrichment).
- RZ1: proposed kinematics with regularization free and zig-zag restricted and equal zero in the boundaries.

Carrera and Ciuffreda [2] addressed the example with several distinct theories but only the layerwise model has been adopted herein as benchmark, which includes both zig-zag effect and interlaminar continuity at each layer interface. The normalized transversal displacement in the center of the square plate is compared with the selected theory in Table 1. A tolerance of 10^{-6} was used in the Newton-Raphson iteration.

Table 1. Normalized displacement $\bar{U}_z$ in the center of the square plate

a/h	4	100
RZ0	2,3846	0,6244
RZ1	3,1351	0,6261
Carrera & Ciuffreda [2]	3,0444	0,6713

From Table 1, the results corresponding to the RZ1 kinematics are closer to the values reported by Carrera and Ciuffreda [2] than those obtained with the RZ0 kinematics, especially for the thick plate. This demonstrates that transverse displacements can be underestimated when the regularization and zig-zag effect are neglected. Figure 3 shows graphical results for normalized shear stress at the mid supported side of the plate and normalized normal stress at the center of the plate.

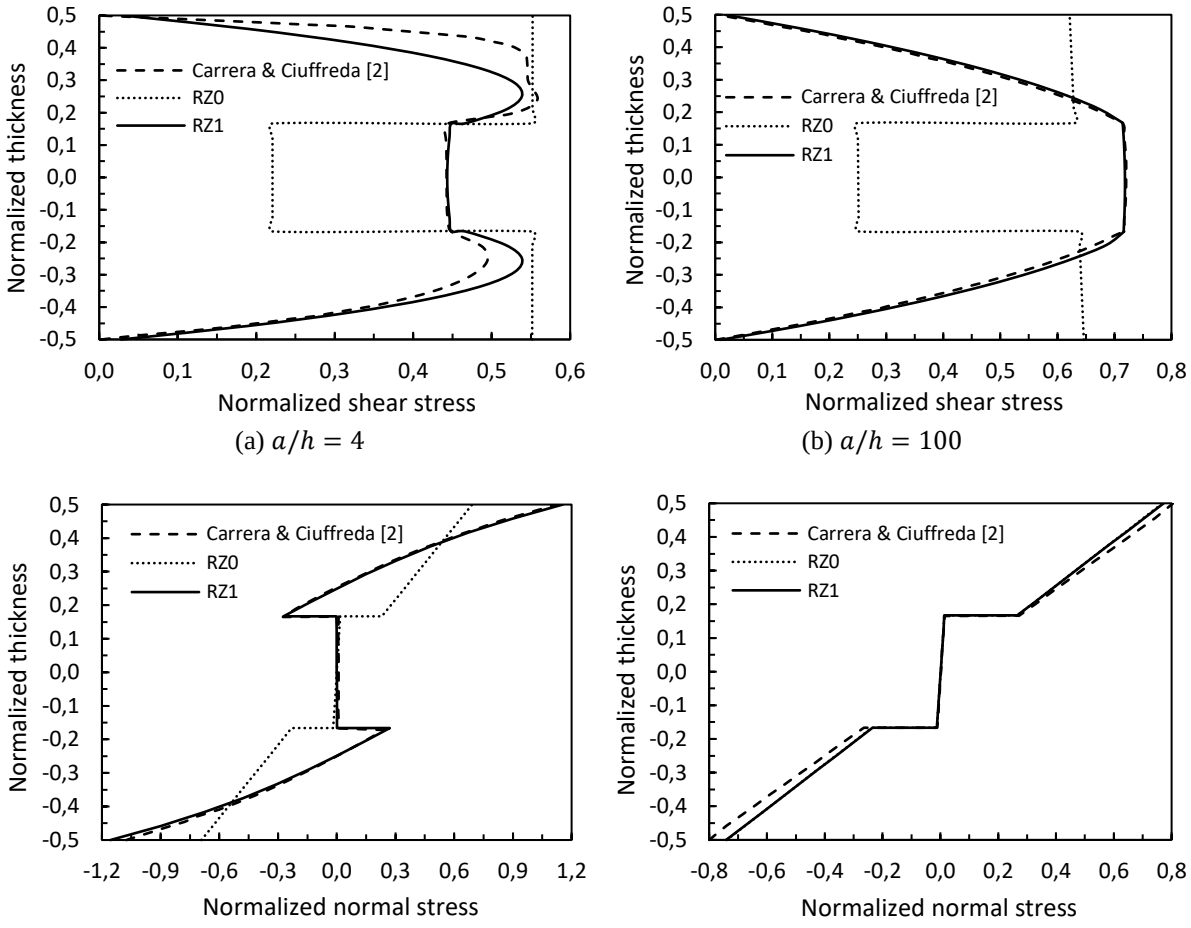

Figure 3. a, b) Normalized shear stress $\bar{\sigma}_{13}$ at coordinates $(0, a/2, \bar{x}_3)$; c, d) Normalized normal stress $\bar{\sigma}_{11}$ at coordinates $(a/2, a/2, \bar{x}_3)$

The influence of the zig-zag effect is more evident in Figure 3. In general, the curves corresponding to RZ1 adhered well to the reference values [2] for both thick and thin plates. As expected, the RZ1 kinematics satisfied the continuity of shear stresses between laminas, while the RZ0 curves are piecewise continuous along the plate thickness. This happens because the RZ0 kinematics is governed by $\tau^k = \gamma^k G^k$, which is able to satisfy the stress continuity solely in lamina *k* without the improvements proposed in the present work.

4 Conclusions

The tested example shows that the proposed formulation regularizes the stress profiles in symmetrical laminates and provides transverse displacements consistent with the reference values. It is worth stressing that the enhanced kinematics uses only 11 degrees of freedom by node, regardless of the number of laminas. Therefore, the proposed nonlinear geometric formulation proved to be efficient and promising for the analysis of symmetric laminated plates and shells. The next step seeks more general applications and to extend the same formulation to asymmetric laminated sections.

Acknowledgements. The authors are grateful for the financial support provided by the Coordenação de Aperfeiçoamento de Pessoal de Nível Superior – Brasil (CAPES) – Grant Finance Code 001.

Authorship statement. The authors hereby confirm that they are the sole liable persons responsible for the authorship of this work, and that all material that has been herein included as part of the present paper is either the property (and authorship) of the authors, or has the permission of the owners to be included here.

References

[1] J. N. Reddy, *Mechanics of laminated composite plates and shells: theory and analysis*. CRC Press, 2. ed., 2004.
[2] E. Carrera and A. Ciuffreda, "A unified formulation to assess theories of multilayered plates for various bending problems". *Composite Structures*, vol. 69, pp. 271–293, 2005.
[3] H. B. Coda, R. R. Paccola and R. Carrazedo, "Zig-Zag effect without degrees of freedom in linear and non linear analysis of laminated plates and shells". *Composite Structures*, vol. 161, pp. 32–50, 2017.
[4] J. Oh, M. Cho and J. Kim, "Buckling analysis of a composite shell with multiple delaminations based on a higher order zig-zag theory". *Finite Elements in Analysis and Design*, vol. 44, pp. 675 – 685, 2008.
[5] N. N. Sy, J. Lee and M. Cho, "Application of the Laplace transformation for the analysis of viscoelastic composite laminates based on equivalent single-layer theories". *International Journal of Aeronautical and Space Sciences*, vol. 13, n. 4, pp. 458–467, 2012.
[6] H. B. Coda, C. C. L-C. Bernardo and R. R. Paccola, "A FEM formulation for the analysis of laminated and functionally graded hyperelastic beams with continuous transverse shear stresses". *Composite Structures*, vol. 292, 2022.
[7] J. Bonet, R. D. Wood, J. Mahaney and P. Heywood, "Finite element analysis of air supported membrane structures". *Computer Methods Applied in Mechanics and Engineering*, vol. 190, pp. 579–595, 2000.
[8] H. B. Coda. *Análise não linear geométrica de sólidos e estruturas: Uma formulação posicional baseada no MEF*. PhD thesis (Tese para concurso de professor titular), Departamento de Engenharia de Estruturas, Escola de Engenharia de São Carlos, Universidade de São Paulo, São Carlos, 2003.
[9] H. B. Coda. *O Método dos elementos finitos posicional: sólidos e estruturas – não linearidade geométrica e dinâmica*. São Carlos: EESC/USP, pp. 284, ISBN 978-85-8023-068-0, 2018.
[10] M. Bischoff and E. Ramm, "Shear deformable shell elements for large strains and rotations". *International Journal for Numerical Methods in Engineering*, vol. 40, n. 23, pp. 4427–4449, 1997.